

# Progress in the Search for the Charge Symmetry Breaking $dd \rightarrow \alpha\pi^0$ Reaction

C. Allgower, A.D. Bacher, J. Doskow, G. East, C. Lavelle, H. Nann, J. Olmsted, R.E. Pollock,  
T. Rinckel, T. Sloan, and E.J. Stephenson  
*Indiana University Cyclotron Facility, Bloomington, IN 47408*

M.A. Pickar  
*Minnesota State University at Mankato, Mankato MN 56002*

P.V. Pancella  
*Western Michigan University, Kalamazoo MI 49001*

A. Smith  
*Hillsdale College, Hillsdale, MI 49242*

J. Rapaport  
*Ohio University, Athens OH 45701*

## *Introduction*

During FY2002, we completed the installation and commissioning of two Pb-glass arrays needed in the search for the charge symmetry breaking  $dd \rightarrow \alpha\pi^0$  reaction. In order to simulate as closely as possible the event characteristics for production running, but with higher statistics, we used  $\pi^0$  decay photons from the  $pd \rightarrow {}^3\text{He}\pi^0$  reaction initiated with a proton beam just above threshold. After the switch of the Cooler beam to deuterons, we made two runs to verify that the luminosity system was working satisfactorily and we found that major revisions were needed in the scintillator configuration. At the same time, we checked running conditions at the highest beam currents available. We determined that the charge symmetry breaking cross section was not large, if it was visible at all. We therefore decided to run  $dd \rightarrow \alpha\pi^0$  production with the higher beam intensities available with the unpolarized deuteron beam. Measurements of the placement of the recoil cone in the channel also suggested that we should lower the energy to 228.5 MeV in order to keep the entire cone within the channel acceptance.

June and July were devoted to production running. Despite being able to obtain good missing mass resolution for the pions from precise time-of-flight measurements for the  ${}^3\text{He}$  nuclei during commissioning, the timing drifts during the longer production runs made this difficult. By making adjustments in replay to the time-of-flight measurements, we obtained a peak with several dozen candidate  $\alpha\pi^0$  events and better, but still poor, missing mass resolution. At this point it was clear that the  $dd \rightarrow \alpha\pi^0$  reaction would have a measurable cross section, that the background from double radiative capture was visible but not a problem, and that spurious events were almost non-existent in the data. In order to verify that the procedures for obtaining the missing mass were working properly, we elected to raise the energy to 231.8 MeV for the July run and to correct for the loss of recoil nuclei that fell outside the channel acceptance. Again, time resolution was an issue. With adjustments, several dozen candidate events were recorded in a missing mass peak located at the pion mass. The July run came to an abrupt end after 9 days of production with the failure of the lower septum magnet windings.

With the remaining week of Cooler running, we switched to the A-region detectors in order to measure the cross section and three analyzing powers for d+d elastic scattering at a beam energy of 231.8 MeV. The polarization was monitored using the known analyzing powers

from d+p elastic scattering [1]. These data will be used to constrain the calculations of the distortions in the d+d channel.

### *Pb-glass and target box installation and commissioning*

During the fall of 2001, the major effort for the setup of the search for the  $dd \rightarrow \alpha\pi^0$  reaction was the exchange of the target box previously used for the tagged neutron experiment for a new one and the subsequent construction of two Pb-glass arrays on either side of the beam line (see Fig. 1 below). The change of target box served two purposes: (1) moving the target point upstream allowed better coverage of the photons from  $\pi^0$  decay, and (2) rearranging the jet target pumping allowed the target box to have two thin aluminum sides so that the photons could emerge with minimal interference. The division of the interior into four pumping stages with a “catcher” for most of the target gas was retained, as were the number of cryo- and turbo-pumps. Provision was included for a beam position monitor just upstream of the jet target and a position-sensitive silicon detector to be used in conjunction with forward plastic scintillators as a luminosity monitor and a measure of the jet target profile.

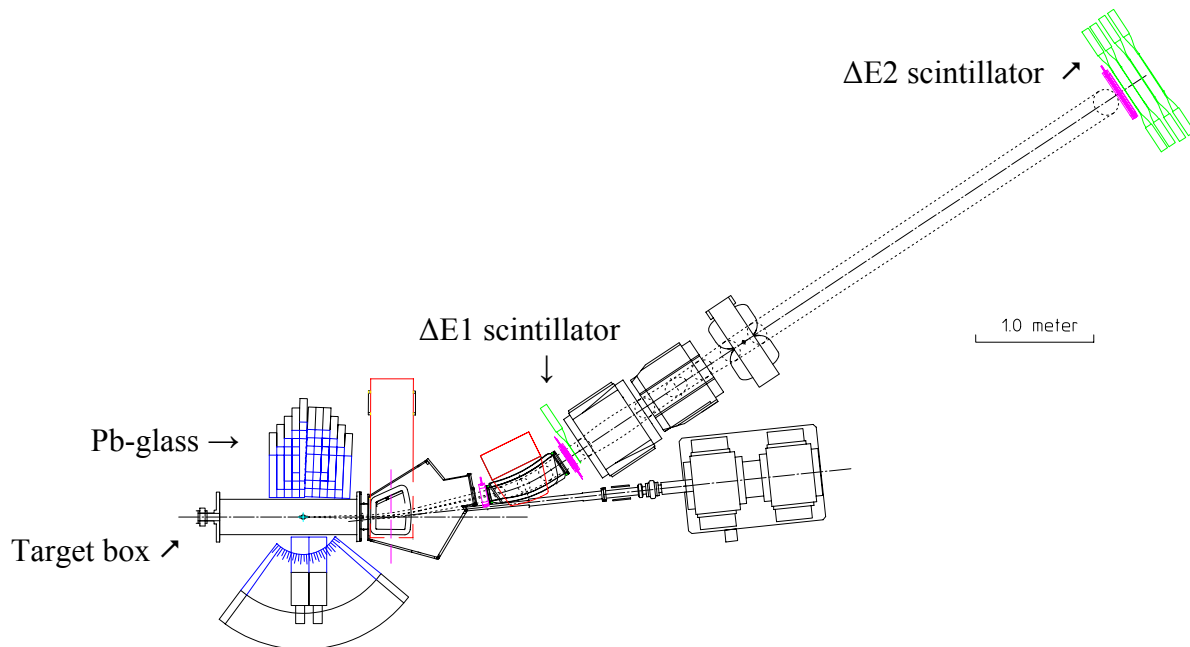


*FIG 1: Layout of the channel including the 6° bending magnet, the target box, and the two Pb-glass arrays.*

The target box was constructed and leak checked before installation into the ring. Two sets of aluminum windows (1/8-inch and 3/16-inch thick) were made for testing to determine the optimum thickness. The 3/16-inch window showed some bowing under pressure, and we decided to stay with this choice for production running. After installation, the apertures that separated the pumping regions were aligned along the beam line. Each had a square opening roughly 2 cm on each side. The jet nozzle was also positioned along the beam line, and a cool-down check was made to verify that it did not move when its temperature was changed. All vacuum pumping was now through ports on the top or bottom of the box.

As part of the modification of the target box region, additional layers of steel were added to the upstream side of the  $6^\circ$  magnet to help minimize the effect of the bending field on the Pb-glass phototubes. The shield then consisted of three steel layers separated by air gaps.

Two tables were constructed for holding the 256 Pb-glass detectors. The support platforms were mounted on ball rods to allow the arrays to be moved away from the target box so that the box could be serviced. The beam-left Pb-glass array consisted of 112 detectors, most of which had a rectangular geometry. While the up- and down-stream columns of detectors, as well as those on the top and bottom rows, were flush with the target box window, those near the center were moved back to give each detector a roughly similar solid angle with respect to the target. The two columns in the center were made with Pb-glass counters available from a previous radiative capture experiment at IUUCF. These were tapered in one dimension and allowed some change in the direction of the other counters so that they pointed more nearly toward the target. Restrictions caused by the windings of the  $6^\circ$  magnet and the magnetic shield caused this array to lose some coverage for the most forward angles. The array on the beam-right side consisted solely of 144 tapered detectors and extended to forward angles near  $30^\circ$ . Each detector was wrapped with mu-metal to reduce the stray magnetic field. Subsequent tests showed that this was not sufficient to protect the most forward phototubes from the field of the  $6^\circ$  magnet, so additional layers of steel were introduced between the original shield and the detectors. The effects of the magnetic field on phototube gain were not completely eliminated, but were kept to a manageable level. On the right-hand side, four larger Pb-glass counters were added to the top and bottom to improve solid angle coverage.

The signal from each Pb-glass photomultiplier base was sent to an amplifier that also provided multiple outputs. One output went to a discriminator. The OR of all discriminator outputs for each array was available for triggering, although it was not used during production running. Sets of 8 signals were multiplexed and sent to a time digitizer.

Two long plastic scintillator paddles were placed across the top and bottom of each of the two Pb-glass arrays in order to provide a coincident trigger for cosmic ray events. These were set up as a separate event stream that could be run during development or production. The cosmic events produced peaks associated with the light generated by high energy muons as they passed through the array. These were used to check the operation and gains of each of the detectors on a regular schedule during running.

The Pb-glass arrays were commissioned using the  $pd \rightarrow {}^3\text{He}\pi^0$  reaction. Data were taken with recoil cone sizes of  $0.95^\circ$  and  $1.55^\circ$ , as well as below threshold. The measurements produced copious numbers of pion events from which the characteristics of the Pb-glass performance can be deduced in replay. While most often the energy was restricted to a single counter, it was common to see it shared with other nearby counters, as shown in Fig. 2. At present, the scheme in place to recover the energy of the original photon involves a search for the counter with the greatest energy, after which the energy of a double ring of detectors around the first is added.

Numerous accidental hits appeared, mostly from the layer of counters that was farthest downstream. It seems likely that these events resulted from photons emitted as the beam struck the mechanical septum between the beam line and the entrance to the channel, about the only place that shows any radioactivity after the beam has been running for a while.



## *Luminosity measurements*

The first system installed for making luminosity measurements consisted of two scintillators mounted at a forward angle of approximately  $3^\circ$  in the laboratory and a position sensitive silicon surface-barrier detector to observe the recoil nuclei from elastic scattering. (This angle was subsequently increased to  $5.3^\circ$  when it was found that many of the recoil events were at too low an energy to trigger the silicon detector.) The two forward scintillators were made thin (0.63 cm) and thick (4.44 cm) in order to provide a  $\Delta E$ -E particle identification capability. Copper absorbers were placed in front of each detector to slow beam energy deuterons to stopping in the second detector. Both the forward scintillators and the silicon detector were mounted at  $57^\circ$  out of the horizontal plane so that the silicon detector and its cooling assembly would be out of the way of photons travelling toward the Pb-glass arrays.

During the Pb-glass commissioning run with the proton beam, very few coincident signals were seen with this system and the patterns in the data were confusing. Later it was determined that the silicon detector had been shadowed by the cooling head that supported the glass nozzle for the jet target system. At this point, we decided that we needed to make drastic changes in the luminosity system. First, the system of forward detectors and position-sensitive silicon detectors would remain, but be positioned at  $24^\circ$  to the horizontal to avoid interference with the cold head. Second, a new system would be built based on detecting d+d elastic scattering at  $90^\circ$  in the center of mass (see Fig. 3 below).

In the design of both of these systems, it was crucial to achieve two objectives. First, the system must measure some reaction that can monitor the luminosity during production running. In both cases, this was d+d elastic scattering. Second, it must be possible to switch to a hydrogen target and make a cross calibration using signals that are distinct from the monitoring reaction. For the forward system, both d+d and d+p elastic scattering give rise to deuterons with nearly the beam energy. The distinction is that for a fixed forward scattering angle, the recoil proton has twice the energy of the recoil deuteron, and this can easily be distinguished in the silicon detector. However, for a system observing d+d scattering at  $\theta_{c.m.} = 90^\circ$ , there is no corresponding d+p coincidence. So additional detectors were placed at  $25^\circ$  in order to see a deuteron at forward angles in coincidence with a proton in one of the side counters. This means that for the second luminosity system, the Pb-glass detectors must be rolled back during the calibration process in order to make room for these new detectors.

In order to improve the diagnostics available with the luminosity system observing d+d elastic scattering at  $90^\circ$ , several features were added, as shown in Fig. 3. The nominally 0.63-cm thick plastic scintillation detector that would be mounted on either side was split into two pieces along a diagonal cut that ranged from 3.5:1 at one end to 1:3.5 at the other. The edges were cut at  $45^\circ$  to provide a cleaner definition of the solid angle. The tapered division produced two signals whose ratio could be used to deduce position horizontally along the scintillator face. With position information on both sides, it became possible for d+d elastic scattering to separate changes in the scattering angle from changes in position of the event origin along the beam z-axis. In order to obtain some information on vertical position of the beam, the two halves were displaced vertically from one another by 0.63 cm each. In order not to be shadowed by the light guide which was connected to the top of each piece, the front half of each pair was raised while the back half lowered. In this way, events that were double coincidences on one side could be checked to see whether they were also double coincidences on the other. If the alignment of the beam and scintillators was perfect, the coplanarity of the two deuterons would require that a

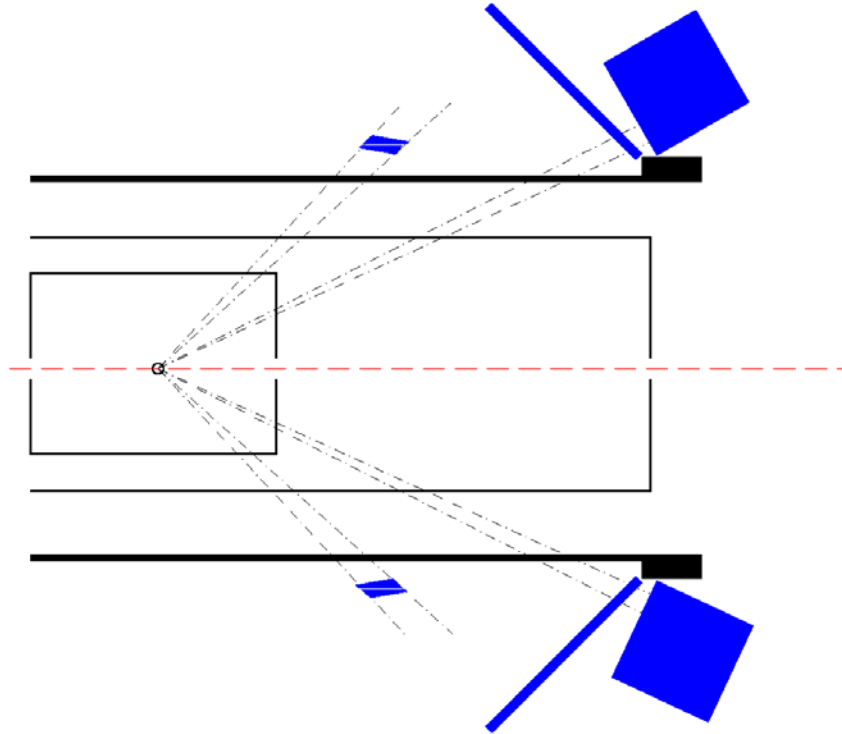


FIG 3. Sketch to scale of the region of the gas jet target and the scintillators used to observe  $d+d$  elastic scattering at  $44^\circ$  on either side and the forward detectors for observing the deuteron from  $d+p$  elastic scattering near  $25^\circ$ . The dash-dot lines indicate the limits of kinematic acceptance for  $d+p$  elastic scattering. The vacuum walls of the target box are shown, along with two layers of internal baffles for the separation of target pumping stages. All of these represent material through which the particles must pass before being detected.

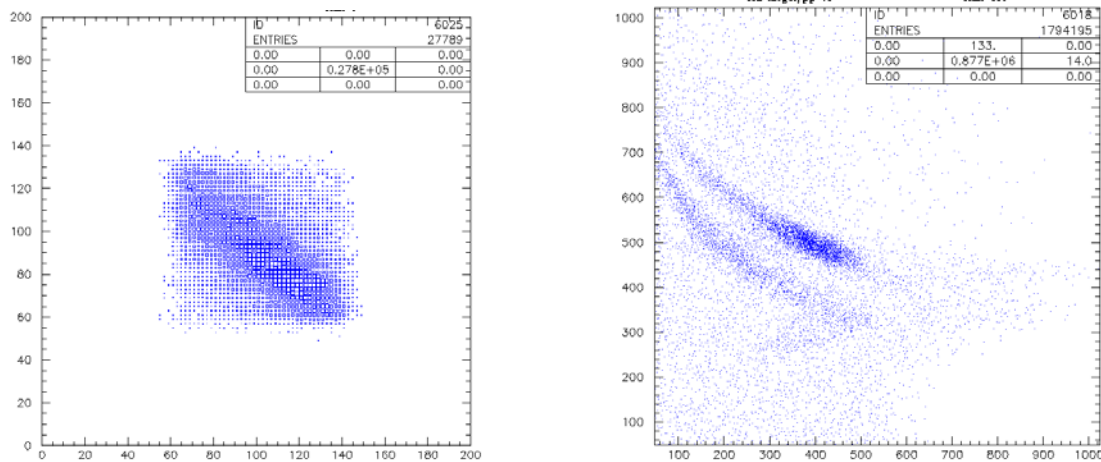


FIG 4: The left panel shows a plot of the left  $44^\circ$  detector position measurement against the right  $44^\circ$  detector position measurement. The ridge through the center is the locus of  $d+d$  elastic scattering events. The right panel shows the pulse height in the  $\Delta E$  detector at  $25^\circ$  against the pulse height in the  $E$  detector. The two loci come from deuterons (upper) and protons (lower) passing through the system.

double hit was always in coincidence with another double hit. The single scintillator of the pair (front or back) that was struck by  $d+d$  events would indicate the direction, and possible magnitude, of any vertical misalignment. However, the scattered particle directions are spread by multiple scattering in the vacuum baffles inside the target box, so quantitative measures of the vertical displacement proved to be difficult.

The new luminosity system performed as expected, as shown by the spectra in Fig. 4. A thin 0.32-cm thick scintillator was added in front of each  $25^\circ$  detector in order to make clean particle identification of the forward-going deuteron (see right panel). The main background throughout this system consisted of breakup protons. Such events were present for all coincident combinations of detectors and required that particle identification work in each case. Thus this second system met the dual requirements of providing a luminosity monitor and a way to calibrate the cross section.

Once it was clear during the short deuteron beam runs that the two luminosity systems were working, the next requirement was that they obtain the same luminosity when run with a pure hydrogen jet. For the newer system, there were two independent measures of the  $d+p$  cross section since there was a  $25^\circ$  and  $44^\circ$  detector on each side. The comparison with the forward system also rested on using known  $d+p$  cross sections since different parts of the angular distribution showed up in each system. Initially, disagreements were large. The worst problem was that the copper absorbers used to make the forward scintillator system a good particle identification system causes large losses from outscattering. Since the elastic peak was large relative to any backgrounds, it was judged important to remove these. Some confusion also arose because of commissioning with a polarized beam that had an unexpected vector polarization. Finally, agreement to within 10% indicated that we were ready to go into production with a working system.

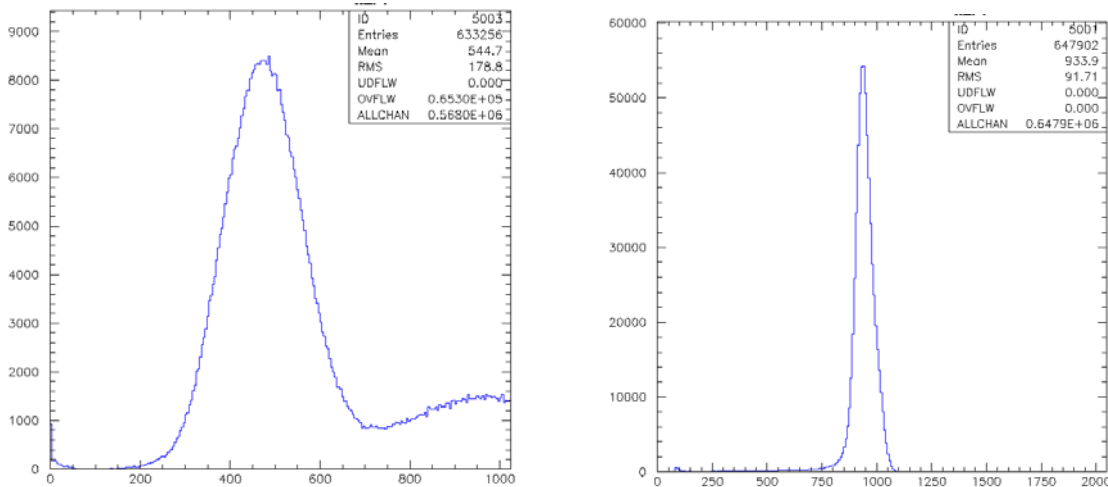


FIG 5: The left panel shows the pulse height spectrum from the silicon detector when HD molecular gas was used as the target. The lower, tall peak comes from recoil deuterium, the higher, incomplete peak is from recoil hydrogen. The relative heights set the ratio of the elastic scattering cross sections for  $d+d$  and  $d+p$  elastic scattering. The right panel shows the  $\Delta E$  scintillator spectrum from the forward detectors in coincidence with the silicon.

## Production running

For each of the two production runs, there was a simple two-part run plan. First, with the Pb-glass detectors rolled back, we would do the cross calibration of the luminosity system using molecular HD gas to observe d+p and d+d elastic scattering simultaneously. The known d+p cross section provided the reference for the luminosity, which in turn set the scale for relating d+d elastic scattering events to the luminosity. Second, we would switch to a deuterium target and put the Pb-glass into position, then commence production running.

For the forward scintillator and silicon detector luminosity calibration, the different parts of the distribution due to hydrogen or deuterium recoils were clear, as seen in Fig. 5. As part of the calibration, runs were made also with H<sub>2</sub> and D<sub>2</sub> targets. From these template shapes, it was possible to obtain the separate contributions from d+p and d+d by adjusting the components in the sum. Likewise, the peak in the right panel illustrates that the elastic scattering group is clean.

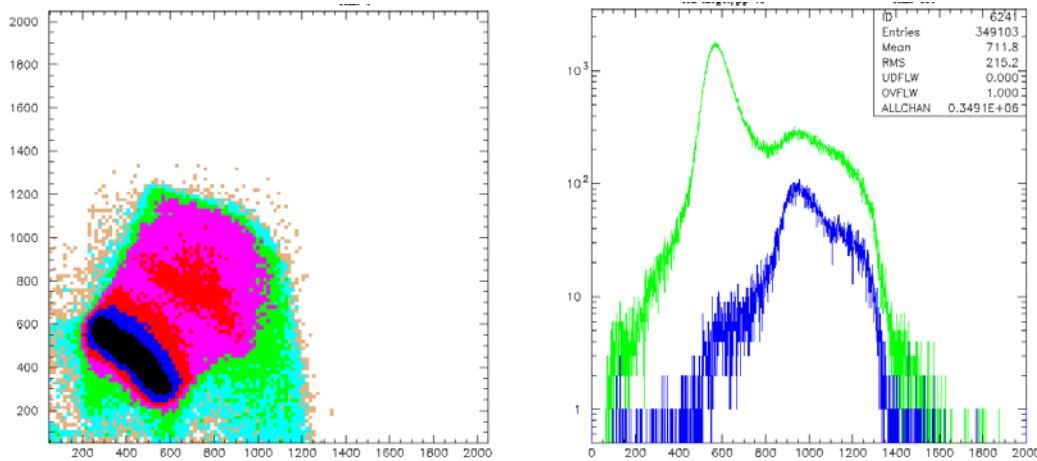


FIG 6: The left panel displays the front against the back pulse height for the left 44° luminosity scintillator pair. The strong diagonal band is from protons, the weaker parallel band at higher pulse height is from deuterons. The fainter plot on the right panel shows the projection onto a diagonal axis of these two particle identification peaks. The smaller spectrum are those events in coincidence with deuterons identified by the opposite 44° detector. There is a peak for the d+d elastic group and a broader distribution from breakup events.

For the combination of 25° and 44° detectors, it was essential to have particle identification spectra for both particles in either the d+d or the d+p elastic scattering groups. For d+p, the forward 25° deuterons were selected from the locus shown in the right panel of Fig. 4. The associated protons appeared in the projected spectra (right panel of Fig. 6) as the larger peak. Additionally, separate windows observed d+d scattering by selecting the deuteron group for each 44° detector pair. Breakup created events with a wide distribution of scintillator pulse heights, and some of these inevitably fell into the windows meant for either d+p or d+d scattering (see right panel of Fig. 6). In order to make a cleaner separation, we also took data with hydrogen and deuterium targets alone. From these data it was possible to determine the extent to which breakup contributed to the rates for either case. Then, with the HD data, a matrix inversion yielded the rates for each elastic scattering component of the target alone.

The calibrations for the June and July runs agreed within a few percent with excellent statistics. Thus the final errors in this process will be almost entirely systematic. One contribution to this error is the uncertainty in the solid angle due to the placement of the two  $44^\circ$  scintillators. A remeasurement of their locations following the July production run has led to new solid angle values that make the two determinations of the luminosity from d+p scattering differ by 30%. At the present time, the losses from multiple scattering have not been estimated. In addition, there is uncertainty in the d+p cross section angular distribution. This is worse for the side scintillator system because the relevant angles for d+p scattering are influenced by three-body effects and this makes it difficult to use Faddeev calculations of the cross section as a reference. Even if the geometrical issues are resolved, the systematic errors will not be a lot lower than this difference because of the uncertainties in the primary cross sections.

Production running was generally smooth. It was necessary to stop about once per day for one to two hours to regenerate the cryopumps that were closest to the gas jet target. At target thicknesses estimated to be about  $3 \times 10^{15} \text{ cm}^{-2}$ , the deuterium gas accumulation quickly made these pumps unserviceable. We stopped less often, but for longer times, to warm the gas jet nozzle to remove material that was clogging the flow. There were occasional pauses for machine issues. The only one of time significance was the heat wave in July that caused the chilled water temperature to rise, making it difficult to maintain operation of all the various systems without overheating.

Identification of candidate events rested on relatively few tests: (1) proper particle identification in the channel scintillators, (2) correct cluster energy and time in each of the two Pb-glass arrays, and (3) a time-of-flight signal in the expected range. Once all three tests were passed, a missing mass calculation was made using the information from the time-of-flight measurement and the position in the first wire chamber (to determine the transverse momentum

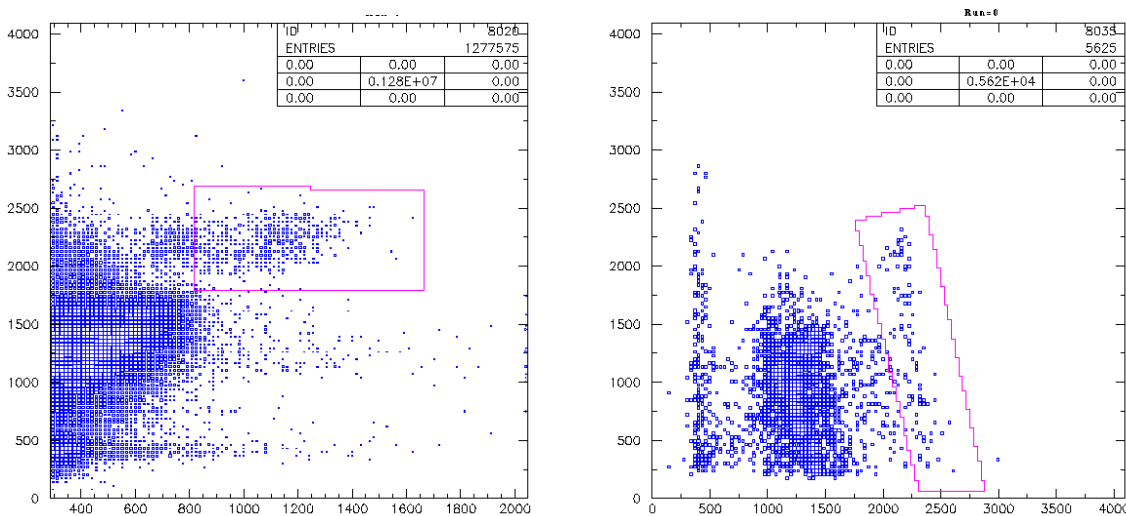
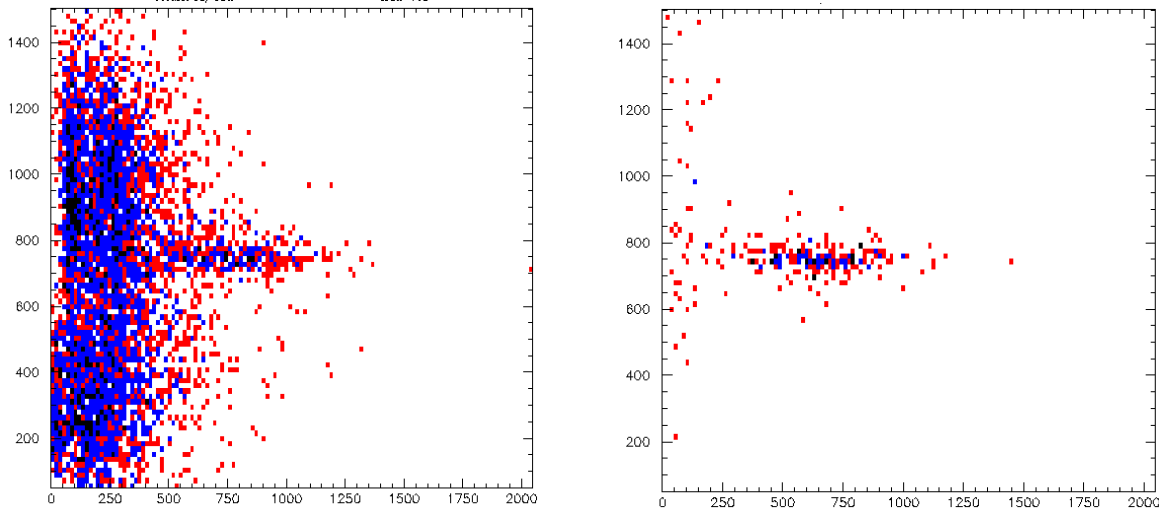


FIG 7: The left panel plots the pulse height for the  $\Delta E2$  scintillator against the pulse height for  $\Delta E1-B$ . The group at the center of the window consists of  $^4\text{He}$  nuclei. The group just at the left edge results from pileup of  $Z=1$  particles. The right panel plots the pulse height for the  $E$  scintillator against the pulse height for  $\Delta E2$ . Again, the window surrounds the locus of  $^4\text{He}$  nuclei. Those events associated with high energy photons seen in the Pb-glass array typically lie near the middle of the locus. These are the data from a single several-hour production run taken in July.

components). The hope was that the distribution in missing mass would help to separate charge symmetry breaking events in which a pion was produced from events that gave rise to two energetic photons through double radiative capture.

Figure 7 shows samples of the selections that are made on channel scintillator pulse height in order to separate  ${}^4\text{He}$  nuclei from the abundance of protons and deuterons that pass down the channel. While not very intense, the  ${}^4\text{He}$  group is sufficiently separate from the  $Z=1$  groups that it can be easily identified in a clear locus. The separation, however, is not completely clean, so other tests for candidate  $\alpha\gamma$  events are needed. The flux of  ${}^4\text{He}$  nuclei are there even with a hydrogen target, so most of them originate from collisions between beam halo and either the walls of the Cooler or residual gas inside the vacuum. Their effective cross section is of the order of several nb, so the requirement to observe high energy photons is essential in the identification of candidate events. The  ${}^4\text{He}$  illumination of the channel appears to be fairly uniform in position and momentum, thus this group will possibly be an aid in checking the acceptance of the channel.



*FIG 8: Two views of the Pb-glass time (corrected for individual counter offset and channel time of flight) against the summed cluster energy for the beam left array. The left panel is gated only on scintillator particle identification in the channel and shows the photon group along with a large random background. The right panel has an additional gate on the high-energy photon group in the opposite Pb-glass array for both time and energy. The two panels have different z-axis scales. These panels show all of the data for the July production run.*

The single most important selection after channel particle identification is the presence of a high-energy photon in one of the two Pb-glass arrays. As shown in Fig. 8, a photon group can be identified by its higher pulse height and time localization. If only a single photon is required for candidate events, however, the separation from random background is impossible for the lower half of the energy spectrum. Only when we require that both arrays record a high-energy photon does the data become clean enough to almost guarantee that there are no background events. Even with a two-photon requirement, there remain a few random events that must be eliminated through an energy cut. It will be important to determine the Pb-glass efficiency when these cuts are applied. Once the requirements for scintillator energy and Pb-glass energy and

time are imposed, an additional wide time-of-flight requirement did not eliminate any of the candidate events.

The transition from commissioning with proton beam to running with deuteron beam involved several crucial changes, all of which had to be correct. It was straightforward to tune the deuteron beam to the correct energy based on the RF frequency used to capture and maintain the beam in the Cooler and the circumference of the ring as measured in the earlier  $pd \rightarrow {}^3\text{He}\pi^0$  calibration run ( $86.786 \pm 0.003$  m). It was also necessary to change the rigidity of the channel. This change was based on energy loss calculations in order to compare  ${}^3\text{He}$  and  ${}^4\text{He}$  rigidities directly for each part of the channel magnetic system. The third change was trigger timing. This was based on a model of the different flight times for real events. The last change involved the algorithm that computes missing mass from time of flight. This algorithm contains a transform between the measured time of flight and the laboratory momentum that is based on the same energy loss model before for channel rigidities. It was assumed in this step that the relative timing information between the detectors upon which the time of flight is based had not changed between proton and deuteron beam running. Indeed, the inputs to the time measuring system branch off at the beginning of the electronics chain and are thus unaffected by changes in the trigger (so long as the time of flight is based on a time difference). Unfortunately, photomultiplier systems are subject to gain shifts as the tubes age and running conditions (such as ambient temperature) change. Compensation for these changes is often necessary so that pulse heights remain in a useful operating range. In addition, there are sometimes other equipment changes that must be done as a part of maintenance. The requirement on time

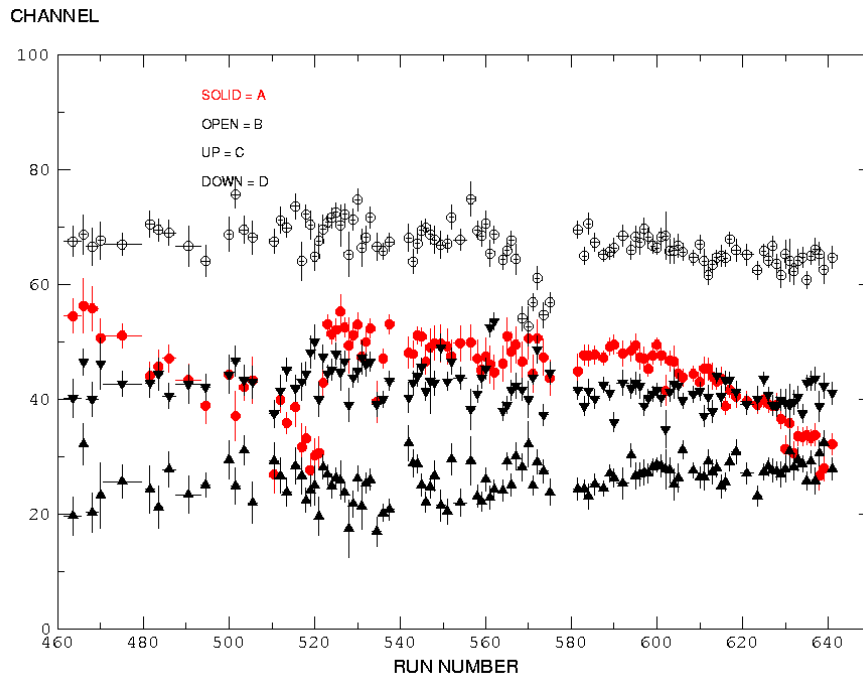


FIG 9: Changing location of the time marker as a function of the run number for the four quadrants of the  $\Delta E1$  scintillator. The errors represent the statistical error in locating the center of the time marker. Sections of these functions were reproduced by polynomials that were then used to subtract away a run dependent correction.

difference stability is much less than one ns. It therefore proved impossible to retain the time of flight settings between the time that the channel was commissioned and the time that production running started.

This time instability required that two steps be taken before it was clear that a useful peak associated with pion production was present in the data. First, the time offset for all photomultipliers with input into the time of flight calculation had to be adjusted. During the June run, several hours of data were taken with the same voltage settings that were used for  $^3\text{He}$  commissioning in order to locate a starting point and to calibrate the time change associated with a phototube bias change. In addition, replay was repeated with a number of different time offsets for the four sections of the  $\Delta E1$  scintillator in order to search for the best missing mass resolution. Small time offset errors tend to spread the missing mass peak first, then move it to lower mass away from the kinematic maximum value. Second, it was clear that for some cases, run-by-run corrections would be needed. For this, a time marker was established with enough statistics to be available for each run. This marker made use of deuterons selected in energy (those that stop in the rear of the E-scintillator) and trajectory (by cutting on a spot in each of the three wire chambers). A sample of the resulting time marker history for the June run is shown below in Fig. 9, where 1 ns is about 21 channels.

With these corrections, it became possible to find a pion peak with a missing mass resolution less than 1 MeV sitting on a background of events associated with double radiative capture. This is the first time that these two processes have been observed unambiguously and separately. (Examples will not be shown here since work on the mass resolution is not complete.) For the June run of 14 days of production, several dozen pion candidate events were identified. At the end of that run, the missing mass resolution still did not offer a clean separation between pion and double radiative capture events in the region between the pion mass and the kinematic maximum at 136.4 MeV. After discussions within the group, we chose to raise the beam energy for the second production run so that such a separation would be clearer with a kinematic maximum at 138.0 MeV. In addition this would provide a second cross section point. From the rate of rise of the cross section with  $\eta$ , the ratio of the pion momentum to its mass, we hoped to determine the relative sizes of S- and P-wave contributions to the cross section.

The July run provided 9 days of production running before the failure of the lower coil in the septum magnet. Time adjustments proved difficult here and good resolution was not achieved until after the end of the run in replay. Again, the resolution was less than 1 MeV. This time, there was a clear group of  $\alpha\gamma\gamma$  double radiative capture events on either side of the peak at levels consistent with the lower energy measurement. Our estimate of the fraction of events lost due to angle acceptance limits of the channel is about 15%.

With so much adjustment being made to the time scale, it is important to have further evidence to confirm that the time information is being handled properly. One method is to look also at the data with only one high energy photon. While helpful in some tough cases, the lack of cleanliness for this cut was often a handicap. At this point there are two other tests, as shown in Fig. 10. One consists of a plot of the missing mass as a function of time of flight (the output versus the input of the algorithm). The correct time offset adjustment will generate a horizontal locus at the pion mass. A small offset in the time will tilt the locus and broaden the missing mass resolution. Such a locus exists in the (2-photon) plot shown on the left below. An additional test is to look for the presence of a circle of greater density at the appropriate place on the XY-1 wire chamber distribution. This is shown at the right in Fig. 9. The center of this

circle is part of the parameter set used to calculate missing mass, and this become one additional check on this system. All of these checks show positive results. Note that the right-hand edge of the circle on XY-1 extends over the edge; these events will be missing from the sample.

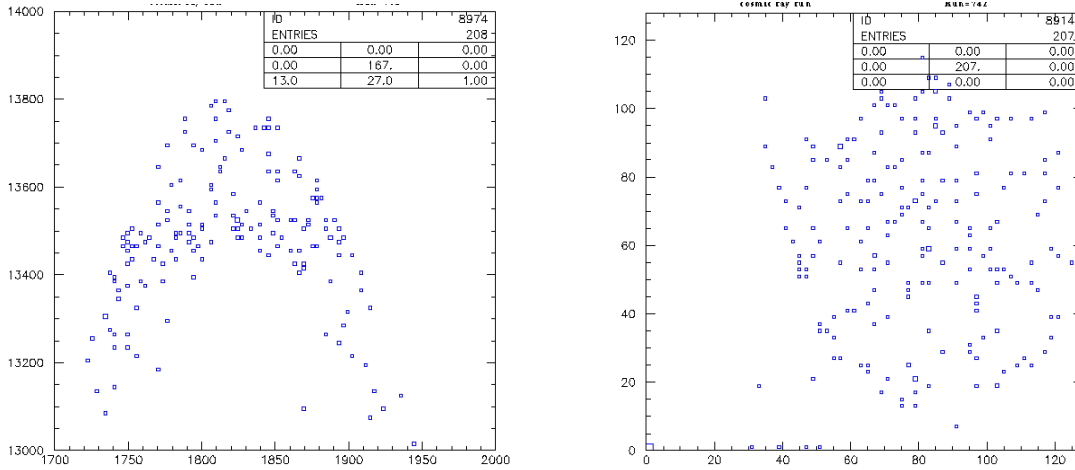


FIG 10: The left panel plots missing mass ( $\times 100$ ) against raw time of flight. The horizontal locus at 135 MeV marks pion events. The right panel shows Y versus X position on the front wire chamber. The number of events is larger inside a roughly circular region. Both panels are gated on scintillator particle identification and the requirement of correct time and energy for two high-energy photons.

The study of these data will continue for some time until the systematic corrections to the cross section are known and errors estimated. Efforts will continue to better understand the time resolution, which is still well above the multiple scattering limit. Most of the effort will go into understanding the systematic effects in the luminosity measurements and the corrections for inefficiencies that will be required in order to quote a correct cross section. The most important part of this will be the estimate of the efficiency of the Pb-glass detectors for 2-photon events (expected to be about 1/3).

### Deuteron-deuteron elastic scattering measurement

At the end of charge symmetry breaking production running, there remained about one week of time available in the Cooler schedule. Since the A-region detectors were still in place (except for the silicon array) and operational, we chose to switch to a measurement of the cross section and analyzing powers for d+d elastic scattering with the hope that at least some measurements could be used to evaluate the approximations used to calculate the distorted waves for the entrance channel to the  $dd \rightarrow \alpha\pi^0$  reaction.

The switch to polarized beam operation took about one day. The BLPL polarimeter was used to check the polarization for four states, as shown in Table I. The V- state is the only one that made use of the less efficient weak field RF transition. For actual operation, a fifth unpolarized state was also included. For the BLPL measurement, this state provided the reference solid angle measurements. For the Cooler, this state is used to determine the azimuthal efficiency of the detector system. With full azimuthal coverage, this arrangement makes possible measurements of the  $iT_{11}$ ,  $T_{20}$ , and  $T_{22}$  analyzing powers.

Table 1: Deuteron Beam Polarizations Measured in BLPL

	$p_y$	$p_{yy}$
vector +	$0.706 \pm 0.049$	$0.832 \pm 0.022$
vector -	$-0.561 \pm 0.049$	$0.602 \pm 0.023$
tensor +	$-0.033 \pm 0.047$	$0.863 \pm 0.022$
tensor -	$-0.121 \pm 0.048$	$-1.558 \pm 0.021$

The PINTEX detectors consist of a forward array that covers laboratory angles from a few degrees out to about  $40^\circ$ . There is a front F scintillator and rear K scintillator that are each divided into 4 quadrants. In between are two multiwire chambers, the first offering XY plane readout and the second UV plane readout. For this experiment, we also installed a barrel of silicon strip detectors that were arranged around the target region. There were 18 detectors arranged in three rings of 6 detector each. Position readout provided additional subdivision in azimuthal angle.

For the elastic scattering study we made use of two targets, hydrogen and deuterium. The hydrogen target provided a reference for the cross section and a known set of analyzing powers for determining the beam polarization. The deuterium, of course, was the target of interest. Half molecular HD gas remained after the charge symmetry breaking calibration, and some of this was used to provide the cross reference for the normalization of the cross section. The most important angular regions for d+p elastic scattering have both the scattered proton and deuteron going into the forward detector array, so one of the two triggers involved two forward prongs. The main background was two forward protons due to deuteron breakup. Some of these events were eliminated from the trigger by requiring that the two prongs be on opposite sides of the beam (using the quadrants from the K scintillator). At the same time, the scattering of two identical particles in d+d elastic scattering requires that one particle be in the forward array and the other in the silicon detectors. This became the second trigger, again with a requirement that the two hits be on opposite sides of the beam. We decided to leave the beam energy at 231.8 MeV where it was at the end of production running for charge symmetry breaking. Despite some restrictions on the two event streams, the number of triggers remained large. Therefore gas pressures inside the target tube were kept small and the beam was of the order of 100-200  $\mu$ A.

During beam setup, checks were made of the vertical beam tune during filling and ramping the Cooler to ensure that the tune stayed away from the depolarizing resonance at  $\nu_y = 0.84$ . During running, the final cuts on d+p elastic scattering were not in place, so it was possible only to verify that the beam polarization in the Cooler ring was large and that the variations followed what was observed for the BLPL polarimeter. Following a calibration with HD gas, production running for d+d elastic scattering ran for 4 days with periodic checks of the polarization using a hydrogen target.

Preliminary conditions were placed that required good wire chamber information, good coplanarity, and a deuteron in the forward and the silicon detectors. A plot of these events as a function of scattering angle shows that modifications to the acceptance for less than full sensitivity to the target exist only for laboratory angles less than about  $12^\circ$  and larger than about  $40^\circ$ . Within these limits, it is possible to identify the downward slope of the single-scattering part of the cross section angular distribution, the break point in slope, and a long region dominated by multiple scattering mechanisms. Beyond these limits, the information on the analyzing powers should still be useful. For some restricted angles, it may be possible to obtain

acceptance corrections from a study of the d+p angular distribution. It is expected that the statistical uncertainties on the analyzing powers will be between 0.01 and 0.02 for angle bins that are as much as  $2^\circ$  wide.

We wish to thank Barbara von Przewoski and Hans-Otto Meyer from the PINTEX collaboration for their assistance with the preparation of this part of our experiment and the use of the PINTEX detectors.

1. K. Sekiguchi *et al.*, Phys. Rev. C **65**, 034003 (2002).